Theoretical Modeling of Associated Structures in Aqueous Solutions of Hydrophobically Modified Telechelic PNIPAM Based on a Neutron Scattering Study

Tsuyoshi Koga,*,† Fumihiko Tanaka,† Ryuhei Motokawa,‡ Satoshi Koizumi,‡ and Françoise M. Winnik§

Department of Polymer Chemistry, Graduate School of Engineering, Kyoto University, Katsura, Kyoto 615-8510, Japan; Soft Matter & Neutron Scattering Group, ASRC, JAEA, Ibaraki 319-1195, Japan; and Department of Chemistry and Faculty of Pharmacy, University of Montréal, CP 6128, Succursale Centre Ville, Montréal QC, Canada H3C 3J7

Received April 28, 2008; Revised Manuscript Received July 5, 2008

ABSTRACT: On the basis of results from a small-angle neutron scattering (SANS) study of aqueous solutions of a telechelic PNIPAM with octadecyl end groups, we developed a theoretical model of the self-assembly of this polymer in water as a function of temperature and concentration. This model leads us to the following description. In solutions of concentration 10 g L^{-1} kept between 10 and 20 °C, telechelic PNIPAMs (M_n = 22 200 g mol^{-1}) associate in the form of flower micelles, containing about 12 polymer chains, assembled in a three-layered core−shell morphology with an inner core consisting of the octadecyl units, a dense inner shell consisting of partly collapsed PNIPAM chains, and an outer shell of swollen hydrated chains. Drastic changes in the scattering profile of the solution heated above 31 °C are attributed to the formation of mesoglobules (diameter of ∼40 nm) consisting of about 1000 polymer chains. On further heating, the aggregation number of the mesoglobules increases. It reaches a value of ∼9000 at 34 °C and stays constant upon further heating. In solutions of lower concentration (1 g L^{-1}), association of flower micelles and mesoglobules does not occur; however, the structure of individual flower micelles and mesoglobules is not affected by the change in concentration. In solutions of 50 g L^{-1} in which flower micelles are expected to be partially connected by bridge chains, a peak attributed to correlation between flower micelles appears in the scattering profiles recorded at low temperature (10−20 °C). In spite of the intermicellar bridging connection, the overall temperature dependence of the scattering profile at 50 g L^{-1} remains similar to that at 10 g L^{-1}. Distinct features of the self-assembled structures formed in aqueous telechelic PNIPAM solutions are discussed in terms of the interactions between water and the polymer main chains.

1. Introduction

Depending on the temperature and on the polymer concentration, associating polymers form a variety of self-assembled structures in water, typical examples of which are flower micelles or physical gels with micellar junctions. The properties of associating polymers have been of great interest, not only because of their scientific importance but also because of their potential applications in diverse fields such as paints, coatings, cosmetics, and drug release formulations.[1−4] Telechelic associating polymers, which consist of a hydrophilic main chain carrying hydrophobic end groups, have been used as typical and simple models of well-defined molecular structure to study their self-assembled structures[5−12] and rheological properties.[13−15] Most of such studies have been carried out under conditions for which the polymer chain is regarded as highly soluble in water, as in the case of hydrophobically modified poly(ethylene oxide) (tel-PEOs), which have been studied in solution by various techniques such as fluorescence spectroscopy[5,6] and small-angle neutron scattering (SANS).[7−9]

Recently, Winnik and co-workers reported the preparation of associative polymers consisting of a poly(*N*-isopropylacrylamide) (PNIPAM) chain carrying alkyl groups at each chain end (tel-PNIPAM) and studied the self-assembled structures and phase behavior in aqueous solutions of tel-PNIPAMs.[16−19] Since the homopolymer PNIPAM is a thermoresponsive polymer, which undergoes a coil-to-globule transition at 32 °C in water,[20] tel-PNIPAMs are expected to exhibit peculiar structural and dynamic properties due to the presence of association between chain ends and the strong temperature sensitivity of the main chain.[21] The phase diagram of the homopolymer PNIPAM was studied by Afroze et al.[22] from the experimental and theoretical points of view by using phenomenological coefficients of the concentration-dependent Flory's χ parameter. Later, Okada et al.[21] proposed a mechanism of cooperative (de)hydration to account for the molecular origin of the temperature sensitivity. By combining this mechanism of cooperative hydration of the main chain with end-chain association, Okada et al.[19] proposed a model that accounts for the downward shift of the cloud-point curves compared to those of the homopolymer. On the basis of the data obtained from light scattering (LS) and fluorescence spectroscopy measurements,[16,18] Kujawa et al. reported that tel-PNIPAMs in cold water show an associative behavior similar to that of typical telechelic associating polymers: formation of flower micelles at low concentrations and network formation by bridging between micelles above a critical concentration. By increasing the temperature, dehydration of the PNIPAM chains takes place, leading to the association of flower micelles at a temperature which is close to the coil-to-globule transition temperature of PNIPAM itself.[18] Although this temperature is far above the cloud point, macroscopic phase separation did not take place, but rather, stable aggregates of narrow size distribution were formed. The aggregates were postulated to be mesoglobules, which have been observed also in dilute solutions of PNIPAM[23] and PNIPAM copolymers.[24,25] The origin of the stability of mesoglobule is still open to discussion.

* To whom correspondence should be addressed.
† Kyoto University.
‡ ASRC, JAEA.
§ University of Montréal.

10.1021/ma800957z CCC: $40.75
Published on Web 11/06/2008

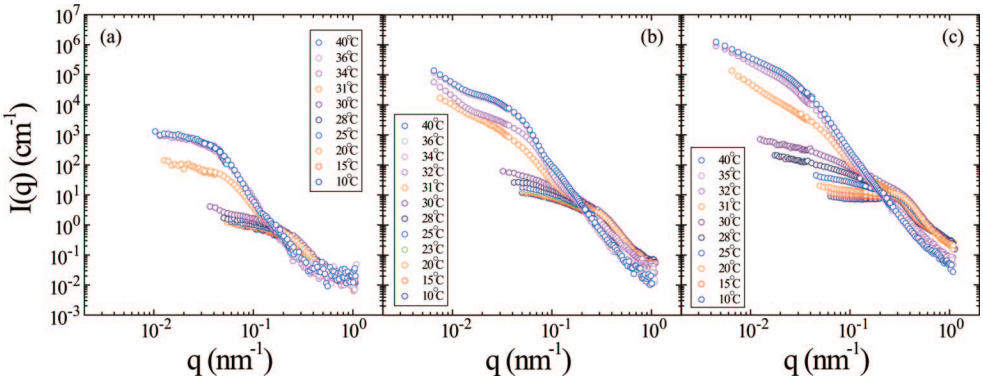

Figure 1. Neutron scattering profiles of tel-PNIPAM in D_2O at (a) 1, (b) 10, and (c) 50 g L^{-1}. Temperature changes from 10 to 40 °C.

It is generally believed to originate from one of the following factors: residual charges at chain termini, partial vitrification of PNIPAM, viscoelastic effects,[25] and electrostatic interactions of charges on the mesoglobule surface.[23]

Koizumi et al.[26] carried out recently a SANS study of solutions of a tel-PNIPAM (M_n = 22 200 g mol^{-1}) using a newly developed small-angle neutron scattering spectrometer with focusing geometry.[27] This instrument achieves a minimum value of measurable wavenumber in the range of a few 10^{-3} nm^{-1}, which corresponds to ultrasmall-angle neutron scattering (USANS) covering a length scale of almost 1 μm in real space. A detailed description of these results will be reported elsewhere. Here we use this SANS study to elaborate a theoretical model of telechelic PNIPAM aqueous solutions as they are heated across their cloud points and across the coil-to-globule transition point of the PNIPAM chain. We consider the various self-assembled structures of tel-PNIPAMs over a wide concentration region (1−50 g L^{-1}) from isolated flower micelles to networks with micellar junctions.

This article presents first a brief summary of the SANS results. This is followed by a description of the theoretical model employed to account for the experimental scattering profiles. By using this model, we scrutinize quantitatively the structures formed in aqueous solutions of tel-PNIPAM as a result of changes in temperature and concentration. We propose a detailed description of the heat-induced progressive transformation of flower micelles into mesoglobules.

2. Experimental Section

2.1. Sample Specimens. The tel-PNIPAM sample (C_{18}-PNIPAM-C_{18}-22K) was synthesized by reversible addition−fragmentation chain transfer (RAFT) polymerization of NIPAM, as described in ref 17. It consists of a PNIPAM chain terminated at each end with an *n*-octadecyl group. The number-averaged molecular weight (M_n = 22 200 g/mol) and polydispersity index (M_w/M_n = 1.16) were determined by gel permeation chromatography (GPC) and proton nuclear magnetic resonance (^{1}H NMR) spectroscopy.[17]

2.2. USANS and SANS Instrument (SANS-J-II). SANS and USANS measurements were carried out with a focusing and polarized neutron ultrasmall-angle neutron scattering spectrometer (SANS-J-II) at JRR3 research reactor (20 MW, Japan Atomic Energy Agency (JAEA), Tokai, Japan).[27,28] Using a disk-type velocity selector[29] provided by the Central Research Institute in Hungary, cold neutrons are monochromated at λ = 6.5 Å with $\Delta\lambda/\lambda$ = 13%, which corresponds to the maximum of Maxwellian wavelength distribution. By changing collimation with respect to the pinhole size and focusing lens, we used either the conventional SANS mode or the focusing USANS mode, which enable us to observe a wide q region from 10^{-3} to 1 nm^{-1}, where q (= $(4\pi/\lambda)$ sin θ) is the magnitude of the scattering vector given by wavelength λ and the scattering angle 2θ. The conventional SANS mode is capable of covering the q regions of $0.03 < q < 0.25$ nm^{-1} and $0.1 < q < 1.5$ nm^{-1} by employing the two sample-to-detector distances 10 and 2.5 m, respectively. The scattered neutrons are detected by a two-dimensional position-sensitive ^{3}He detector of 0.58 m diameter and 5 mm resolution. The data were corrected first for counting efficiency and then for instrumental background including air scattering. After circular averaging, the scattering was converted to differential scattering cross section in absolute units (cm^{-1}), using a secondary standard of irradiated Al plate. Incoherent scattering from hydrogen was subtracted as the background by using a reference sample of H_2O.

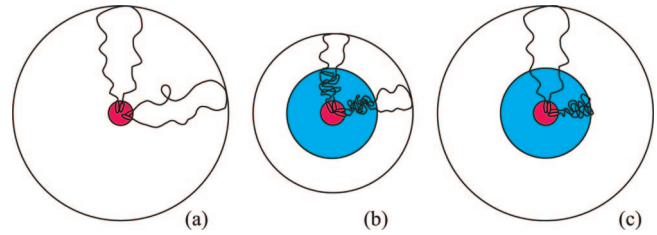

Figure 2. Core−shell models for flower micelles. The conformation of PNIPAM chains in each micelle is schematically drawn. The red circle represents the core consisting of the octadecyl units. (a) Two-layered core−shell model. (b) Three-layered core−shell model with all PNIPAM chains collapsed near the core. (c) Three-layered core−shell model in which the collapsed and swollen PNIPAM chains coexist near the core.

The focusing USANS mode is capable of reaching the lower q region of $0.003 < q < 0.04$ nm^{-1} by using a compound lens made of MgF_2 and a high-resolution cross-wired position sensitive photomultiplier R3239 (5 in. size and 0.5 mm resolution, provided by Hamamatsu Photonics Co. Ltd.) with a ZnS/^{6}LiF scintillator. The compound lens, designed by National Institute of Standard and Technology (NIST),[30] was a biconcave MgF_2 crystal (provided by Ohyo Koken Kogyo Co. Ltd., Japan) with a diameter of 30 mm, a radius of curvature of 25 mm, and a thickness in the center of 1 mm. Lenses (70 pieces) were placed before the sample position along the beam path. The overall transmission is about 50%. USANS was calibrated in absolute intensity units (cm^{-1}) by comparing to SANS, which was already calibrated by using an irradiated Al plate a secondary standard.

2.3. Sample Preparation for USANS and SANS Measurements. Polymer solutions in D_2O (1, 10, and 50 g L^{-1}) were kept at 5 °C for 2 weeks prior to measurements to ensure solution homogeneity. Solutions were placed in a quartz cell (1−2 mm thick and 17 mm wide), which typically gives a transmission of ca. 70%. The temperature of the sample analyzed was controlled by circulating water. It was heated from 10 to 40 °C as follows: the solution was brought to a given temperature in small increments (1−5 °C); it was kept at this temperature for 30 min prior to measurement. SANS data accumulation took approximately 3−4 h. The sample was then brought to a higher temperature and subjected to the same treatment. Overall, a complete temperature study took ~48 h. SANS data were not collected upon cooling the

solutions due to beam time limitations. Thus, we were unable to assess the reversibility of all the transformations. There is experimental evidence such that heating−cooling cycle presents a hysteresis due to the irreversibility of intra- and intermolecular hydrogen bonds in the case of the homopolymer[31] and telechelic PNIPAMs.[18]

3. Summary of the Experimental Results

In this section, we present an overview of the temperature and concentration dependence of the SANS profiles.[26] Detailed analyses of these profiles will be given in the following sections. The overall SANS data obtained for solutions of 1, 10, and 50 g L^{-1} are shown in Figure 1. Focusing on the data of the solution 10 g L^{-1}, we note that, at low temperature far below the coil-to-globule transition temperature, PNIPAM chains are swollen by hydration, while the octadecyl groups aggregate to form the core of micelles by hydrophobic effects. The main contribution to the SANS intensity originates from such flower micelles at 10 °C. The scattering profile stays almost unchanged from 10 to 20 °C. Above 20 °C, the scattering intensity in the low q region ($q < 0.2$ nm^{-1}) increases with temperature, indicating association of the micelles. According to previous experiments,[18] the cloud point of this solution lies around 25 °C, yet there is no significant change in the scattering profile at this temperature.

At 31 °C, however, the scattering profile drastically changes. There appears a hump at $q \simeq 0.05$ nm^{-1}, which indicates that large aggregates of about 100 nm in size are formed. They are considered to be "mesoglobules".[23,24] Moreover, there is excess scattering exhibiting a power law in the small q region ($q <$ 0.02 nm^{-1}), implying the formation of larger objects via association of mesoglobules.

In the case of the solutions of low concentration (1 g L^{-1}), the scattering profile at 10 °C is almost the same as that of 10 g L^{-1} (see Figure 14 for details). The growth of the scattering profile in the small q region between 20 and 30 °C is less pronounced than that at 10 g L^{-1}. Moreover, there is no excess scattering in the data above 31 °C at 1 g L^{-1}. These findings suggest that the association of micelles or mesoglobules is suppressed in solutions of such low concentration.

The overall temperature dependence of the scattering profile recorded for a solution of 50 g L^{-1} is similar to that of 10 g L^{-1} as shown in Figure 1, except for the appearance of a peak in solution well below the cloud point due to the correlation between flower micelles.

4. Theoretical Modeling

In this section, we construct theoretical models to interpret the experimental SANS data. We start from the definition

$$I(q) = \left\langle \sum_{i,j} b_i b_j e^{-i\mathbf{q}\mathbf{r}_{ij}} \right\rangle \tag{4.1}$$

for the scattering function, where $\mathbf{q}$ is the scattering vector, $\mathbf{r}_{ij} \equiv \mathbf{r}_i - \mathbf{r}_j$ ($\mathbf{r}_i$ is the position vector of the ith element) and b_i is its scattering length. In what follows, we mainly focus on the data at 10 g L^{-1}. Since the form of the SANS profile changes with temperature due to the formation of higher order structures, we first consider the lowest temperature 10 °C and then move to higher temperatures.

4.1. Model of Flower Micelles. We begin with the data for 10 g L^{-1} at 10 °C (Figure 3). At this temperature, the main contribution to the scattering profile originates from individual flower micelle the formation of which was demonstrated in a previous study.[18] In the low q region, the scattering profile in Figure 3 is however somewhat different from the simple summation of individual flower micelles in that it gradually increases with decreasing wavenumber. We tried to use the conventional core−shell model shown schematically in Figure 2a, which has been often used for star polymers and polymeric micelles.[9,32,33] The result of this model shown in Figure 3 (green line) is almost constant in the region of $q < R_s^{-1}$ and rapidly decreases with q at $q \simeq R_s^{-1}$, where R_s is the radius of the micelle (in Figure 3a, $R_s \simeq 15$ nm). Although we can adjust R_s to get a better fit in the narrow range around $q \simeq 0.3$ nm^{-1}, the whole behavior of the scattering data cannot be described by such a simple model.

To improve the fit of the model to the experimental data, we introduce a middle layer in the model. We consider that the PNIPAM chains may partially collapse near the core due to dehydration induced in part by the hydrophobic effect of the end group and in part by the high monomer density close to the core. As a result, there is a region around the core where the density of PNIPAM chains is much higher than that in the shell region. We call it the middle region. The density profile of the tel-PNIPAMs is hence described by a three-layered core−shell model consisting of the core, middle, and shell regions, as shown in Figure 2b,c.

It is important to point here that a similar sharp density change in the profile of PNIPAM chains was proposed to interpret experimental observations related to the collapse of PNIPAM chains grafted on a flat surface.[34,35] On the basis of the *n*-cluster model,[36] Wagner et al.[37] predicted a vertical phase separation of the brushes. The appearance of a sharp density change in the profile of PNIPAM chains grafted from a flat surface as a function of the distance from the surface was studied also by Baulin et al.[38] by using the free energy obtained by Afroze et al.[22] We found here a similar sharp density profile as a function of the radial distance from the core of the micelles. We expect that the vertical separation can exist also in flower micelles with dense core in spite of the effect of the curvature.

Let f be the aggregation number of a micelle in terms of tel-PNIPAM chains. The core region consists of $2f$ close-packed octadecyl groups. The density is then given by $\rho_c(r) =$ constant ($r < R_c$). The middle region contains a number $N_{NIPAM}^{(m)}$ of monomer units and water molecules. The density profile in the middle region is assumed to be constant: $\rho_m(r) =$ constant ($R_c < r < R_m$). The shell region consists of swollen chains and water, and it has $N_{NIPAM}^{(s)}$ NIPAM monomer units. The density profile is assumed to be described by the Daoud−Cotton model for star polymers[32] and polymeric micelles:[39]

$$\rho_s(r) \sim r^{-(3\nu-1)/\nu} \tag{4.2}$$

for $R_m < r < R_s$, where $\nu = 3/5$ is the Flory exponent for a swollen chain.

The scattering intensity from flower micelles is given by the sum of the contribution from each micelle[40]

$$I(q) = n_{mic}\overline{I_{mic}(q)} \tag{4.3}$$

Since the micelles are polydisperse, we have taken the average $\overline{\cdots}$ over the distribution of the aggregation number. The number density of micelles n_{mic} is given by $cN_A/\bar{f}M_w$ (N_A being Avogadro's number), and $I_{mic}(q)$ is the scattering function of a single flower micelle. It can be decomposed into two parts: the average density profile and the fluctuation around it:

$$I_{mic}(q) = AI_{cs}(q) + I_b(q) \tag{4.4}$$

where $I_{cs}(q)$ is the squared average density profile of the three-layer core−shell model and $I_b(q)$ comes from the density fluctuations inside the micelle. A is a correction factor to be specified later.

The scattering function $I_{cs}(q)$ of the average density in the three-layer model with core (c), middle layer (m), and shell (s) is written as[41]

$$I_{cs}(q) = F_{cs}(q)^2 \tag{4.5}$$

where F_{cs} has three parts:

$$F_{cs}(q) = F_c(q) + F_m(q) + F_s(q) \tag{4.6}$$

each being given by

$$F_\alpha(q) = b_\alpha \int_{R_\beta}^{R_\alpha} \rho_\alpha(r) \frac{\sin qr}{qr} r^2 \, dr / \int_{R_\beta}^{R_\alpha} \rho_\alpha(r) r^2 \, dr \tag{4.7}$$

for three layers α = c, m, s. The lower limit R_β of the integrals are defined by $R_\beta = 0$ for α = c, $R_\beta = R_c$ for α = m, and $R_\beta = R_m$ for α = s. Similarly, the scattering length b_α of the α region is given by

$$b_c = 2f b_{C18} \tag{4.8}$$

$$b_m = N_{NIPAM}^{(m)} b_{NIPAM} \tag{4.9}$$

$$b_s = N_{NIPAM}^{(s)} b_{NIPAM} \tag{4.10}$$

where the scattering lengths of the octadecyl group and NIPAM units are known to be $b_{C18} = -3.68 \times 10^{-11}$ cm^{-1} and $b_{NIPAM} = -9.47 \times 10^{-12}$ cm^{-1}.[42]

The second term $I_b(q)$ in eq 4.4 from the density fluctuations in a micelle is introduced to account for the behavior of the scattering profile at large $q > 0.5$ nm^{-1}, where the scattering profile obeys a power law as shown in Figure 3. The density fluctuations inside the micelle region can be expressed by the blob picture of semidilute polymer solutions.[43] Since the scattering by the density fluctuations depends on the conformation of polymers, we consider the contribution from the middle and shell regions separately. The α-region consists of $n_b^{(\alpha)}$ blobs of size $\xi^{(\alpha)}$.[44] There are $N_b^{(\alpha)} \simeq (\xi^{(\alpha)}/l_{NIPAM})^{\nu^{(\alpha)}}$ segments in a blob, where $\nu^{(\alpha)}$ is the exponent related to the polymer dimension in the α-region ($\nu^{(s)} = 3/5$ for a swollen chain and $\nu^{(m)} = 1/3$ for collapsed chain), and l_{NIPAM} is the length of the NIPAM units. The scattering function from the density fluctuations is then given by

$$I_b(q) = \sum_\alpha n_b^{(\alpha)} b_{NIPAM}^2 N_b^{(\alpha)2} P_b(q, \alpha) \tag{4.11}$$

where

$$P_b(q, \alpha) = \frac{1}{q\xi^{(\alpha)}} \frac{\sin(\mu^{(\alpha)} \tan^{-1}(q\xi^{(\alpha)}))}{\mu^{(\alpha)}[1 + (q\xi^{(\alpha)})^2]^{\mu^{(\alpha)}/2}} \tag{4.12}$$

with $\mu^{(\alpha)} \equiv 1/\nu^{(\alpha)} - 1$ is the form factor of the blobs in α-region.

The amplitude A in eq 4.4 is determined to ensure the normalization condition $I_{mic}(q \to 0) = (N b_{NIPAM} + 2b_{C18})^2 f^2$. From eqs 4.11 and 4.4, we find

$$A = (N b_{NIPAM} + 2b_{C18})^2 f^2 - \sum_\alpha n_b^{(\alpha)} b_{NIPAM}^2 N_b^{(\alpha)2} \tag{4.13}$$

In order to choose model parameters consistent with the molecular structure, we consider the conformation of the PNIPAM chains in a flower micelle. The simplest model for the conformation of the PNIPAM chains is shown in Figure 2b, where all the PNIPAM chains of a micelle collapse near the core. However, by careful fitting, we noticed that the shell region of this model was too thin to fit the experimental data as shown in Figure 3. To improve this defect, we assume that the collapsed and swollen NIPAM chains coexist in a micelle as shown in Figure 2c. This assumption led to a shell radius large enough to reproduce the scattering profile as shown in Figure 3. Applying this model to the data in Figure 3, we find the average aggregation number of flower micelles to be $\bar{f} = 12$. When taking the average in eq 4.3, we assume that the distribution of the aggregation number f of micelles is Gaussian with the standard deviation σ_f. It is chosen to be $\sigma_f = 0.15\bar{f}$ by fitting. We also take into account the instrumental smearing effects using a resolution function. Details of the parameters obtained by the analysis will be discussed in section 5.

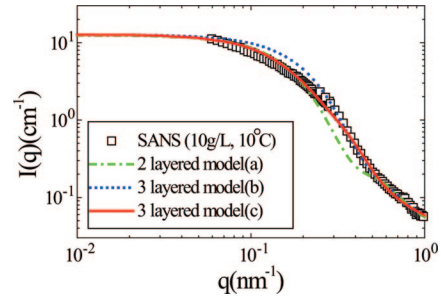

Figure 3. Scattering function obtained by the three models (a)−(c) shown in Figure 2.

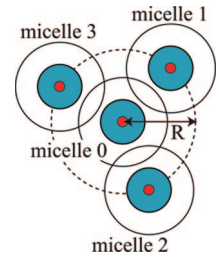

Figure 4. A model of aggregates consisting of M micelles (M = 4).

4.2. Scattering Function of Micellar Aggregates. As the temperature is increased above 20 °C, the scattering profile in the low q region is gradually enhanced compared to the high q region, as shown in Figure 5. This change in profile is indicative of the association of flower micelles. We propose the simple model shown in Figure 4 to describe the micellar aggregates consisting of M flower micelles (M-mers). We focus on one micelle (micelle 0) whose position is fixed at the origin. Micelles associated with it are randomly distributed on a sphere of radius R. Overlap of the micelles on the sphere is ignored. We then employ the general decomposing procedure [(A.6) in the Appendix] and find

$$I(q) = n_M \overline{I_{agg}(q)} \tag{4.14}$$

where $\overline{\cdots}$ is the average over the distribution of the aggregation number, $n_M = n_{mic}/M$ is the number density of the M-mers, and

$$I_{agg}(q) = M\overline{I_{mic}(q)} + 2(M-1)\overline{F_{cs}(q)}^2 \frac{\sin qR}{qR} + (M-1)(M-2)\left[\overline{F_{cs}(q)} \frac{\sin qR}{qR}\right]^2 \tag{4.15}$$

By comparison with the experimental data shown in Figure 5, we find that the model proposed above leads to a good fit. We have adjusted the parameters using $\bar{f} = 12$ as a fixed value. We also take into account the polydispersity in the aggregation number M and in the distance R between micelles to suppress oscillations of the scattering curves. The former is given by the Schulz−Zimm distribution function[45,46] with the standard devia-

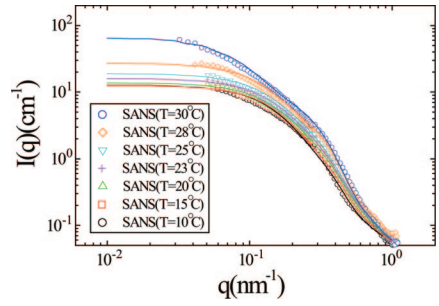

Figure 5. Comparison between the experimental data and results by the model eq 4.14 in the temperature range 10−30 °C.

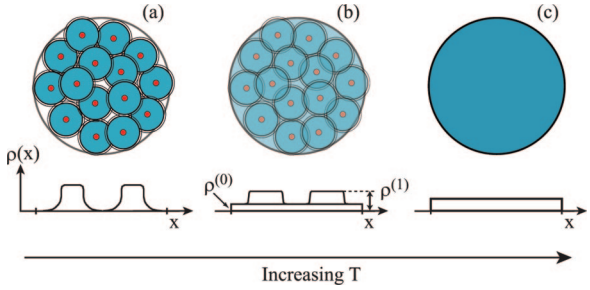

Figure 6. Schematic figure of a mesoglobule consisting of micelles (a) and the dissociation of micelles in a mesoglobule with increasing temperature (b, c). The lower part shows the schematic density profiles.

tion $\bar{M}/\sqrt{10}$, while the latter is assumed to be Gaussian with the mean value $\bar{R} = 2.5R_m$, the standard deviation $\sigma_R = 0.08\bar{R}$ for $T < 30$ °C, and $\bar{R} = 3R_m$, $\sigma_R = 0.3\bar{R}$ for $T = 30$ °C. The parameters obtained by this analysis characterize the structure of the aggregates and will be discussed in the next section.

4.3. Model of Mesoglobules. As discussed in section 3, the scattering profile drastically changes for solutions heated above 31 °C. The characteristic feature of high-temperature profile is the presence of a hump at $q \simeq 0.05$ nm^{-1} ascribed to the formation of mesoglobules. It is important to note that the contribution from individual micelles is also observed at $q = 0.2-0.5$ nm^{-1}, so that each mesoglobule must consist of many micelles as shown in Figure 6a. The scattering from the micelles becomes less prominent for solutions at 32 °C and completely disappears above 34 °C. This indicates that with increasing temperature the micelles dissociate and merge within each mesoglobule.

First, we construct a model for mesoglobules without considering the dissociation of micelles (Figure 6a). We assume that a mesoglobule forms a sphere of radius R_{mg} consisting of N_{mg} micelles. The general procedure (A.6) in the Appendix leads to

$$I_{mg}^{(1)}(q) = N_{mg}\overline{I_{mic}(q)} + N_{mg}\overline{F_{cs}(q)}^2[S_{mg}(q) - 1] \quad (4.16)$$

$$S_{mg}(q) = 1 + (N_{mg} - 1)P_{sph}(x_{mg}) \quad (4.17)$$

for the scattering function of a mesoglobule with undissociated micelles, where $x_{mg} \equiv qR_{mg}$ is the dimensionless scattering wavenumber. Since a mesoglobule is assumed to be a sphere of radius R_{mg}, $S_{mg}(q)$ is represented by the form factor of a sphere, $P_{sph}(x) \equiv F_{sph}(x)^2$, where

$$F_{sph}(x) = \frac{3}{x^3}(\sin x - x\cos x) \quad (4.18)$$

To take the dissociation of micelles into consideration, we assume that a number g of polymer chains are dissolved and dispersed in a mesoglobule, while the rest $f = f_0 - g$ of the polymer chains remain in micellar form as schematically shown in Figure 6. The scattering function of a single mesoglobule of this model is shown to take the form

$$I_{mg}(q) = I_{mg}^{(1)}(q) + 2b_p N_{mg}{}^2 g P_{sph}(x_{mg})\overline{F_{cs}(q)} + (b_p N_{mg} g)^2 P_{sph}(x_{mg}) \quad (4.19)$$

where b_p is the scattering length of one polymer chain defined by

$$b_p = Nb_{NIPAM} + 2b_{C18} \quad (4.20)$$

If the micelles are not dissociated ($g = 0$), eq 4.19 reduces to the previous result eq 4.16:

$$I_{mg}(q) = I_{mg}^{(1)}(q) \quad (4.21)$$

In contrast, if micelles completely dissociate in mesoglobules ($f = 0$) as shown in Figure 6c, eq 4.19 reduces to the scattering function of an isolated sphere:

$$I_{mg}(q) = (b_p N_{mg} g)^2 P_{sph}(x_{mg}) \quad (4.22)$$

Therefore, we have an extrapolation formula covering the two limits. Although we assumed that the hydrophobic core of the micelles dissociates in the mesoglobules, we cannot directly prove it because the scattering contrast of the octadecyl unit is not sufficiently strong. Since the scattering intensity from the micelles becomes small in the temperature range 31−34 °C, we think this assumption plausible. Previous fluorescence studies on the solutions of PNIPAM copolymers carrying hydrophobic alkylpyrenylacrylamides[47] provided experimental evidence for the presence of hydrophobic microdomains below the LCST and for their disruption at the LCST. In order to assess the fate of the micelles in mesoglobule, contrast-variation SANS measurements need to be performed.

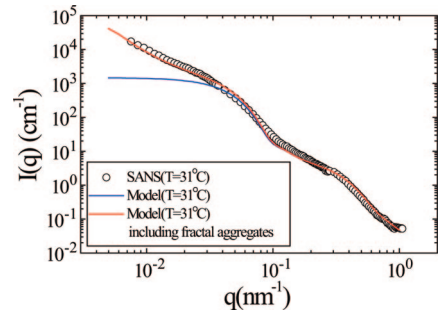

Figure 7. Comparison between the SANS data (31 °C) and results by the model eqs 4.23 and 4.24.

Since we have the number density of mesoglobule $n_{mg} = n_{mic}/\overline{N_{mg}}$, the scattering function of the whole system is given by

$$I(q) = n_{mg}\overline{I_{mg}(q)} \quad (4.23)$$

In order to take the size distribution of mesoglobules into account, we average $I_{mg}(q)$ over the distribution of the aggregation number N_{mg} of mesoglobules counted in terms of micelles. It is again assumed to be Gaussian with the standard deviation $\sigma_{mg} = 0.5\overline{N_{mg}}$. We also assume that the distributions of f and N_{mg} are independent of each other. In Figure 7, we present a comparison of eq 4.23 with the experimental data. In the calculation, the parameters were determined for $f_0 = 12$. We also assume that there is no corona region in the flower micelles above 31 °C. For $q > 0.05$ nm^{-1}, the scattering profile is well

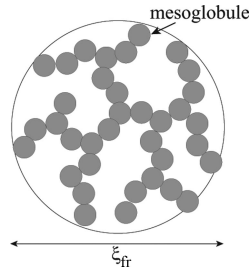

Figure 8. Schematic figure of a fractal aggregate consisting of mesoglobules.

described by the model with $\bar{f}/f_0 = 0.67$. The radius of a mesoglobule is about $R_{mg} \simeq 45$ nm, a value giving the hump at $q = 0.05$ nm^{-1} in the scattering profile. For $q < 0.05$ nm^{-1}, the experimental scattering curves are enhanced. We discuss its physical origin in the next subsection.

4.4. Aggregates of Mesoglobule. Let us focus on the small q region above 31 °C. The power law q^{-a} ($a \simeq 2$) of the intensity in the double-logarithmic plot suggests that mesoglobules form fractal aggregates with a fractal dimension $D_f = 2$ as shown in Figure 8. Let N_{fr} be the number of mesoglobules forming a fractal aggregate, and let ξ_{fr} be its correlation length. By applying the procedure (A.6) again, the scattering function of a fractal is given by

$$I(q) = n_{fr} I_{fr}(q) \tag{4.24}$$

where

$$I_{fr}(q) = N_{fr}\overline{I_{mg}(q)} + N_{fr}\overline{F_{mg}(q)}^2[S_{fr}(q) - 1] \tag{4.25}$$

and

$$F_{mg}(q) = b_p N_{mg}(f + g)F_{sph}(x_{mg}) \tag{4.26}$$

$$S_{fr}(q) = 1 + (N_{fr} - 1)P_{fr}(x_{fr}) \tag{4.27}$$

where the number density of fractal aggregates is $n_{fr} = n_{mg}/N_{fr}$ and $x_{fr} \equiv q\xi_{fr}$. The scattering function of a fractal aggregate $P_{fr}(x)$ is given by[41]

$$P_{fr}(x) = \frac{1}{D_f - 1}\frac{1}{x[1 + x^2]^{(D_f-1)/2}} \sin[(D_f - 1)\tan^{-1}(x)] \tag{4.28}$$

The scattering amplitude $\overline{F_{mg}(q)}$ of mesoglobules in eq 4.25 is obtained by averaging over the size distribution of the mesoglobules as in the case of $I_{mg}(q)$. In Figure 7, we draw a red line including the contribution of fractals and compared with the experiments. Comparison with the experimental data at other temperatures is shown in Figure 9. For solutions at 32 °C, we obtain $\bar{f}/f_0 = 0.42$. This means that 58% of the polymer chains in a micelle are dissolved in a mesoglobule. In the case of solutions at 34 °C, we assume that flower micelles completely dissociate in the mesoglobule, i.e., $f = 0$. Details of the parameters obtained from this analysis will be discussed in the next section.

5. Discussion

5.1. Effect of Temperature. In Figure 10, the fraction $N^{(m)}_{NIPAM}/Nf$ of NIPAM monomer units in the middle layer and their volume fraction are plotted against temperature below 30 °C. The fraction $N^{(m)}_{NIPAM}$ increases with temperature due to the dehydration of the chains. Simultaneously, the volume fraction of the polymer chains in the middle layer also increases because water molecules are squeezed out of the middle region. As a result, the size R_m of the middle region stays almost constant in the temperature range covering 10−30 °C. In contrast, the radius of the shell region R_s rapidly decreases with temperature (Figure 11). The radius of gyration $R_G^{(mic)}$ of a micelle and R_G of the micellar aggregates below 30 °C are plotted in Figure 12. The size $R_G^{(mic)}$ of each micelle decreases with temperature, which is consistent with previous results, while the radius R_G increases, indicating that with increasing temperature further association takes place.

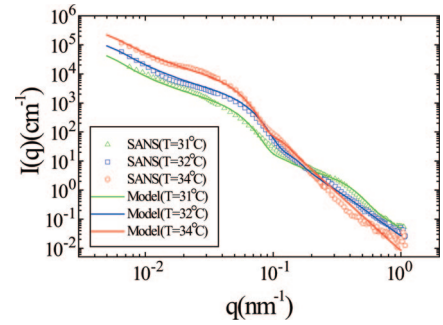

Figure 9. Comparison between the SANS data (31−34 °C) and results by the model eq 4.24 at 31−34 °C.

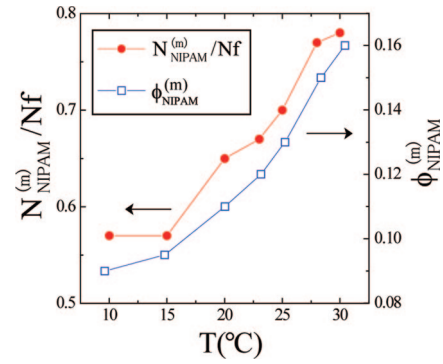

Figure 10. Temperature dependence of the number $N^{(m)}_{NIPAM}$ of polymer chains collapsed in the middle region and of the volume fraction $\phi^{(m)}_{NIPAM}$ of polymers in the middle region.

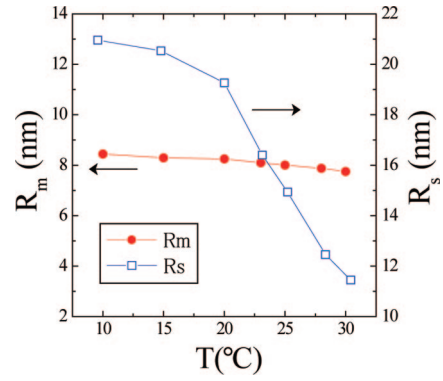

Figure 11. Temperature dependence of the radii R_m and R_s between T = 10−30 °C.

Solutions of the same polymer sample have been analyzed previously by light scattering (LS). The radius of gyration of flower micelles obtained by LS is larger than that obtained by SANS analysis given in Figure 12. For example, R_G was determined to be 35 nm at $T = 20$ °C for 10 g L^{-1} by LS,[18] a value more than 3 times as large as $R_G \simeq 11$ nm at $T = 20$ °C derived from SANS. Moreover, the aggregation number $N_{agg} \simeq 32$ of micelle found by LS is much larger than that by SANS ($N_{agg} \simeq 12$).

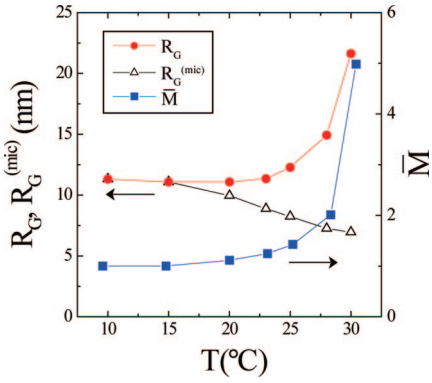

Figure 12. Temperature dependences of the radius of gyration of micelle aggregates, R_G, and of single micelle, $R_G^{(mic)}$, together with the aggregation number M of micelles.

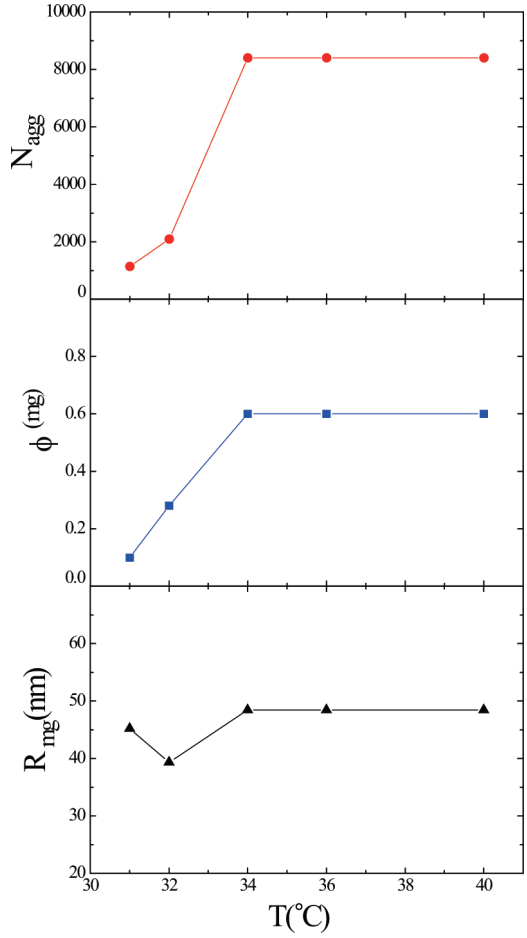

Figure 13. Temperature dependence of the aggregation number N_{agg} of polymers in a mesoglobule (a), the volume fraction $\phi^{(mg)}$ of polymers in the mesoglobule (b), and the radius R_{mg} of a mesoglobule (c).

Several causes may lead to the differences between SANS and LS. First, we have to consider the fact that the measurable wavenumber by LS is smaller than that by SANS. Therefore, if the LS data contain the contribution from large micellar aggregates, which are not detected by SANS, the size estimated from the LS data becomes larger than that of a single micelle obtained by SANS. Actually, a recent LS study[48] on a tel-PNIPAM showed that association of flower micelles occurs in solutions below 10 g L^{-1} at 25 °C. It is interesting to note that the values of R_G and N_{agg} for single micelle estimated by extrapolation of the LS data[48] is almost consistent with those by SANS.

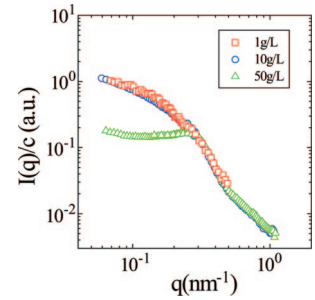

Figure 14. Concentration dependence of the scattering profiles normalized by the concentration at 10 °C.

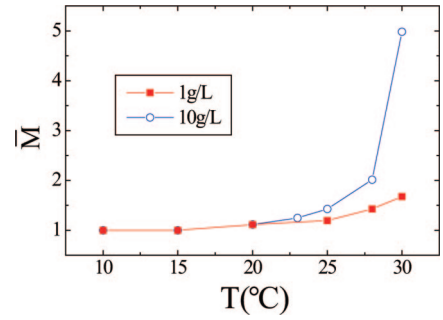

Figure 15. Temperature dependence of the aggregation number of micelles in the range 10−30 °C.

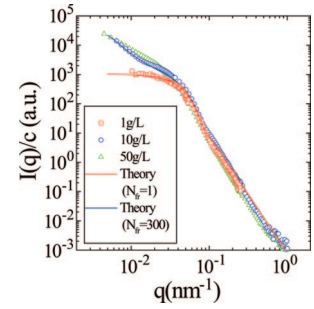

Figure 16. Concentration dependence of the scattering profiles at 40 °C normalized by the concentration. The fractal model with $N_{fr} = 1$ and 300 are also shown (solid lines).

Another important effect to consider is the deuterium isotope effect. Light scattering experiments were carried out with solutions in H_2O, whereas D_2O was the solvent in SANS experiments. According to previous studies,[49,50] the coil-to-globule transition temperature of the homopolymer PNIPAM in D_2O is higher by about 2 °C compared to that in H_2O. Therefore, we should compare the data at 20 °C in H_2O with those at 22 °C in D_2O. The SANS data show that association of flower micelles takes place above 20 °C, which may account for the discrepancy between the LS and SANS experimental results. However, the radius of gyration and the aggregation number of micellar aggregates at 22 °C by SANS estimated from the data in Figure 12 are much smaller than those by LS in H_2O.

Another factor that may be considered is the fact that PNIPAM chains are believed to be more extended in D_2O than in H_2O for solutions far below the coil-to-globule transition temperature.[49] This effect is expected to enhance the stability of flower micelles and suppress their association in D_2O. Thus, the association of flower micelles in D_2O may not take place to as large an extent as in H_2O, as a consequence of the steric effect created by polymer chains which are more extended in D_2O than in H_2O. It would be interesting to study associated

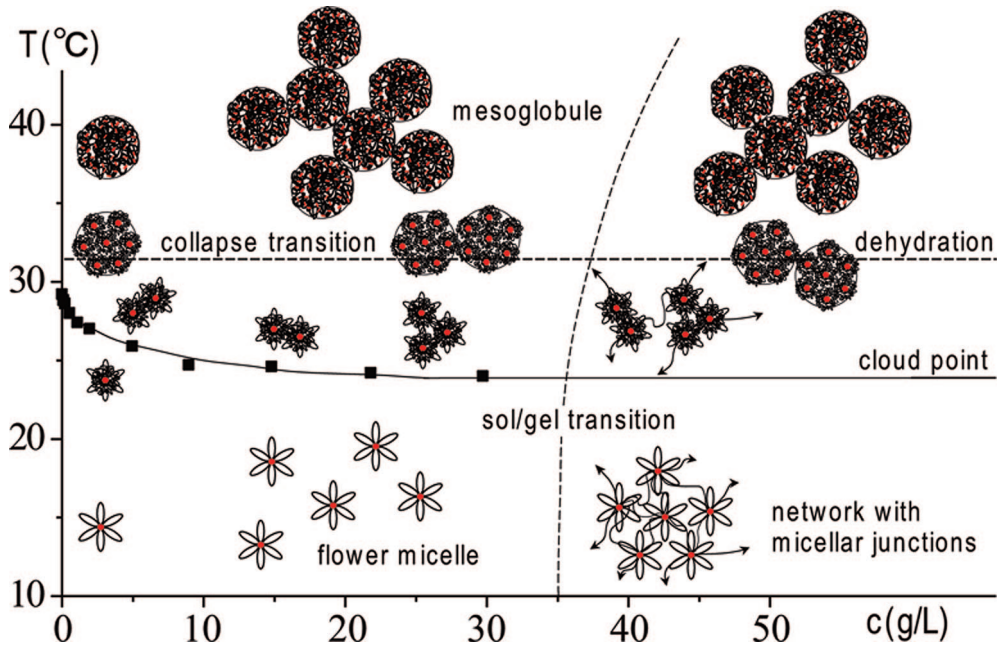

Figure 17. Temperature−concentration phase diagram of telechelic PNIPAM in water. It schematically shows collapse transition temperature (broken line), cloud-point line (solid line), and sol/gel transition line (broken line) together with associated structures such as flower micelles, mesoglobules, flowers connected by bridge chains, and aggregates of mesoglobules.

structures of the tel-PNIPAM in D_2O by LS and compare the results with those by SANS.

In the high-temperature region, mesoglobules form. The temperature dependence of the mesoglobule aggregation number N_{agg} (in terms of the number of polymer chains per mesoglobule), the volume fraction $\phi^{(mg)}$ of polymers in the mesoglobules, and the mesoglobule radius R_{mg} is presented in Figure 13. The aggregation number N_{agg} increases with temperature from 31 to 34 °C. Simultaneously, the volume fraction also increases as water molecules are expelled from the mesoglobules. As a result, the size of the mesoglobule remains nearly constant in this temperature region.

Since the scattering profiles do not change above 34 °C, the parameters deduced from them are also independent of temperature.

As the coil-to-globule transition proceeds, water molecules bound to the PNIPAM chains are released and squeezed out to the bulk. Then the volume fraction of polymers in the mesoglobule becomes large, leading to very slow dynamics of concentration fluctuations within the mesoglobules such that the structure becomes almost frozen at 34 °C.

Mesoglobules formed in dilute solutions of the homopolymer PNIPAM above the coil-to-globule transition temperature have been studied previously by neutron scattering.[23] The size of PNIPAM mesoglobules was shown to decrease with temperature, a tendency different from that depicted in Figure 13. It should be noted however that in the study of homopolymer PNIPAM the scattering intensities were observed only in the Porod's regime. The form factor of the mesoglobules could not be determined because of the narrow q range (from 0.04 to 0.4 nm^{-1}) of the experimental data. To obtain a definite conclusion, it would be necessary to carry out SANS measurements of PNIPAM solutions over a wide q region.

5.2. Effect of the Polymer Concentration. Scattering profiles recorded in the low-temperature region, normalized by the polymer concentration of 1, 10, and 50 g L^{-1} at 10 °C, are presented in Figure 14. The plot for the solution of 1 g L^{-1} is almost identical to that for 10 g L^{-1}, implying that the structure of the micelles is independent of the concentration between 1 and 10 g L^{-1}. Hence, the number of micelles in solutions of 1 g L^{-1} is 1/10 that in solutions of 10 g L^{-1}.

For the solution of 50 g L^{-1}, the scattering profile presents a peak at $q_{max} = 0.25$ nm^{-1} due to the correlation between different flower micelles.[51] From the peak position, the distance l between micelles is roughly estimated as $l \simeq 2\pi/q_{max} \simeq 24$ nm, leading to $f \simeq cN_A l^3/M_w \simeq 19$ for the aggregation number f of micelles. Although this value is somewhat larger than $f = 12$ obtained in the more dilute regions (1 and 10 g L^{-1}), the result ($f \simeq 19$) does not differ so much. Moreover, since the scattering profile in the large q region ($q > 0.25$ nm) for solutions of 50 g L^{-1} agrees well with that for solutions of 10 g L^{-1}, the internal structure of micelles is believed to be almost the same from 10 to 50 g L^{-1}.

In the 10−30 °C, the average aggregation number remains constant up to 20 °C and gradually increases with temperature as shown in Figure 15. Above 20 °C, the aggregation number for the 1 g L^{-1} solution is smaller than that of 10 g L^{-1}.

The scattering data in the high-temperature range normalized by the concentration are presented in Figure 16 and compared with the theoretical model eq 4.24 with $N_{fr} = 1$ with other parameters being the same as those for 10 g L^{-1}. The scattering profiles at 1 g L^{-1} have no excess scattering at $q < 0.03$ nm^{-1}. This behavior is also observed in the scattering profiles above 31 °C at 1 g L^{-1} as shown in Figure 1a. Since the excess scattering at small q is interpreted as the contribution of associated mesoglobules, the SANS data indicate that association of mesoglobules does not take place at 1 g L^{-1}. The good agreement between the data and theory implies that the structure of mesoglobules is the same as that at 10 g L^{-1}.

For 50 g L^{-1}, the scattering profile at $q > 0.05$ nm^{-1} is almost the same, indicating that the structure of mesoglobules is nearly identical. The intensity in the small $q < 0.05$ nm^{-1} region is slightly larger than that for 10 g L^{-1}, implying that association of mesoglobules at 50 g L^{-1} is more pronounced compared to 10 g L^{-1}. We thus find that at high temperatures the structure of mesoglobules formed is independent of concentration, whereas the association of the mesoglobules depends on concentration.

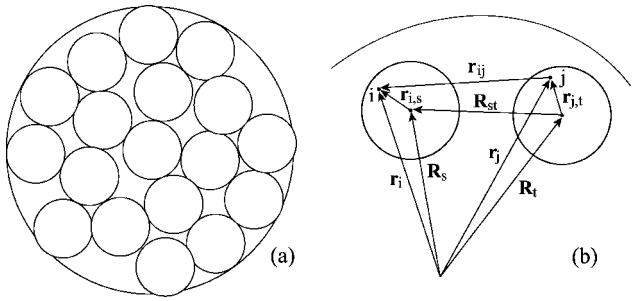

Figure 18. Schematic figure of an aggregate consisting of many elements.

6. Conclusion

We have constructed a theoretical model to account for the temperature and concentration dependence of SANS profiles recorded for solutions of telechelic PNIPAM. This model led us to propose a consistent description of the self-assembled structures of telechelic PNIPAM in D_2O over wide temperature and concentration ranges. A pictorial representation of the temperature−concentration dependence of the solutions is given in Figure 17. Telechelic PNIPAMs associate in the form of flower micelles in dilute solutions at low temperatures. On heating, collapse of PNIPAM chain by dehydration starts near the core of the flower micelles and eventually leads to association of micelles. The temperature sensitivity was attributed to the dehydration of the chain which takes place cooperatively due to the correlation between neighboring bound water molecules.[21] Flower micelles were described by a three-layered core−shell structure by analogy to the vertical phase separation observed and modeled in the case of grafted PNPAM chains.[34,35,37,38] This study provides the first experimental evidence of the occurrence of this kind of phenomenon in flower micelle of tel-PNIPAM. Moreover, the scattering profiles recorded above 31 °C unambiguously indicate the presence of isolated mesoglobules already reported in the case of dilute PNIPAM solutions.[23−25] The mesoglobules remain stable far above the cloud point, although the hydrophobic cores of individual micelles may not be preserved within each mesoglobule. We determined here for the first time the form factor of mesoglobule by employing the focusing SANS method (Figure 16). We also clearly showed that mesoglobules consist of many flower micelles near the transition point (31 °C). The effect of molecular weight on associative behavior of tel-PNIPAMs has already been studied by LS.[18] It would be interesting to study the M_w effect by SANS as well.

In solutions of high concentrations, we have observed a peak in the scattering profile attributed to correlation between flower micelles even at low temperature, which can be interpreted by the packing of micelles. The effects of such network formation cannot be assessed by static SANS experiments. However, the rheological properties of micellar networks are expected to be much different from those of dense un-cross-linked micellar solutions.

Acknowledgment. We thank Dr. P. Kujawa for critical reading of the manuscript and for valuable comments. We acknowledge the partial support of this work by a Grant-in-Aid for Scientific Research (B) from the Japan Society for the Promotion of Science under Grant No. 19350057.

Appendix. A Derivation of Scattering Functions

In this appendix, we briefly describe a general procedure to decompose the scattering function from an aggregate into intra- and intercorrelation. It is assumed to consist of the number N of identical elements as shown in Figure 18a.

Let the vector $\mathbf{r}_{ij}$ in Figure 18b be defined by

$$\mathbf{r}_i - \mathbf{r}_j = \mathbf{r}_{i,s} - \mathbf{r}_{j,t} + \mathbf{R}_s - \mathbf{R}_t \tag{A.1}$$

where $\mathbf{r}_{i,s} \equiv \mathbf{r}_i - \mathbf{R}_s$ is the position vector of $\mathbf{r}_i$ relative to the center $\mathbf{R}_s$ of mass of the sth element. The scattering function can then be approximately given by

$$I(q) = N\left\langle \sum_{i,j} b_i b_j e^{-i\mathbf{q}\cdot\mathbf{r}_{ij}} \right\rangle + \sum_{s\neq t} \sum_{i}^{(s)} \sum_{j}^{(t)} \langle b_i e^{-i\mathbf{q}\cdot\mathbf{r}_{i,s}} \rangle \langle b_j e^{i\mathbf{q}\cdot\mathbf{r}_{j,t}} \rangle \langle e^{-i\mathbf{q}\cdot\mathbf{R}_{st}} \rangle \tag{A.2}$$

The first term gives the correlation within an element, while the second term gives interelement correlation. To write in a compact way, let

$$I^{(\mathrm{iso})}(q) = \left\langle \sum_{i,j} b_i b_j e^{-i\mathbf{q}\cdot\mathbf{r}_{ij}} \right\rangle \tag{A.3}$$

$$F(q) = \left\langle \sum_{i}^{(s)} b_i e^{-i\mathbf{q}\cdot\mathbf{r}_{i,s}} \right\rangle \tag{A.4}$$

be the scattering function and amplitude from a single element, and let

$$S(q) = \frac{1}{N} \sum_{s,t} \langle e^{-i\mathbf{q}\cdot\mathbf{R}_{st}} \rangle = 1 + \frac{1}{N} \sum_{s\neq t} \langle e^{-i\mathbf{q}\cdot\mathbf{R}_{st}} \rangle \tag{A.5}$$

be the correlation function (structure factor) between a pair of the elements. Then, eq A.2 can be written as

$$I(q) = NI^{(\mathrm{iso})}(q) + NF(q)^2[S(q) - 1] \tag{A.6}$$

We can apply this decoupling approximation to several different length scales of association. The scattering functions for mesoglobules, eq 4.16, and their aggregates, eq 4.25, are obtained by a straightforward application of eq A.6.

In the case of micelle aggregates shown in Figure 4, the summation in eq A.2 is written as follows:

$$\left\langle \sum_{s\neq t} e^{-i\mathbf{q}\cdot\mathbf{R}_{st}} \right\rangle \simeq 2(M-1)\frac{\sin qR}{qR} + (M-1)(M-2)\left[\frac{\sin qR}{qR}\right]^2 \tag{A.7}$$

Substituting eqs 4.4, 4.5, and A.7 into eq A.2, we obtain eq 4.15.

References and Notes

(1) *Hydrophilic Polymers: Performance with Environmental Acceptability*; Glass, J. E., Ed.; American Chemical Society: Washington, DC, **1996**; Vol. *248*.
(2) *Associative Polymers in Aqueous Solution*; Glass, J. E., Ed.; American Chemical Society: Washington, DC, 2000; Vol. *765*.
(3) *Amphiphilic Block Copolymers: Self-Assembly and Applications*; Alexandridis, P., Lindman, B., Eds.; Elsevier: New York, 2000.
(4) Winnik, M. A.; Yekta, A. *Curr. Opin. Colloid Interface Sci.* **1997**, *2*, 424.
(5) Yekta, A.; Duhamel, J.; Adiwidjaja, H.; Brochard, P.; Winnik, M. A. *Langmuir* **1993**, *9*, 881.
(6) Yekta, A.; Xu, B.; Duhamel, J.; Adiwidjaja, H.; Winnik, M. A. *Macromolecules* **1995**, *28*, 956.
(7) Séréro, Y.; Aznar, R.; Porte, G.; Berret, J.-F.; Calvet, D.; Collet, A.; Viguier, M. *Phys. Rev. Lett.* **1998**, *81*, 5584.
(8) Séréro, Y.; Jacobsen, V.; Berret, J.-F.; May, R. *Macromolecules* **2000**, *33*, 1841.
(9) Beaudoin, E.; Borisov, O.; Lapp, A.; Billon, L.; Hiorns, R. C.; Francois, J. *Macromolecules* **2002**, *35*, 7436.

(10) Witten, T. A. *J. Phys. (Paris)* **1988**, *49*, 1055.
(11) Milner, S. T.; Witten, T. A. *Macromolecules* **1992**, *25*, 5495.
(12) Semenov, A. N.; Rubinstein, M. *Macromolecules* **1998**, *31*, 1373.
(13) Annable, T.; Buscall, R.; Ettelaie, R.; Whittlestone, D. *J. Rheol.* **1993**, *37*, 695.
(14) (a) Berret, J.-F.; Séréro, Y.; Winkelman, B.; Calvet, D.; Collet, A.; Viguier, M. *J. Rheol.* **2001**, *45*, 477. (b) Berret, J.-F.; Séréro, Y. *Phys. Rev. Lett.* **2001**, *87*, 048303.
(15) Ma, S. X.; Cooper, S. L. *Macromolecules* **2001**, *34*, 3294.
(16) Kujawa, P.; Watanabe, H.; Tanaka, F.; Winnik, F. M. *Eur. Phys. J. E* **2005**, *17*, 129.
(17) Kujawa, P.; Segui, F.; Shaban, S.; Diab, C.; Okada, Y.; Tanaka, F.; Winnik, F. M. *Macromolecules* **2006**, *39*, 341.
(18) Kujawa, P.; Tanaka, F.; Winnik, F. M. *Macromolecules* **2006**, *39*, 3048.
(19) Okada, Y.; Tanaka, F.; Kujawa, P.; Winnik, F. M. *J. Chem. Phys.* **2006**, *125*, 244902.
(20) Schild, H. G. *Prog. Polym. Sci.* **1992**, *17*, 163.
(21) Okada, Y.; Tanaka, F. *Macromolecules* **2005**, *38*, 4465.
(22) Afroze, F.; Nies, E.; Berghmans, H. J. *Mol. Struct.* **2000**, *554*, 55.
(23) Balu, C.; Delsanti, M.; Guenoun, P.; Monti, F.; Cloitre, M. *Langmuir* **2007**, *23*, 2404.
(24) Zhang, G.; Wu, C. *Adv. Polym. Sci.* **2006**, *195*, 101, and references therein.
(25) Aseyev, V. O.; Tenhu, H.; Winnik, F. M. *Adv. Polym. Sci.* **2006**, *196*, 1, and references therein.
(26) Motokawa, R.; Koizumi, S.; Koga, T.; Tanaka, F.; Winnik, F. M. Manuscript in preparation.
(27) Koizumi, S.; Iwase, H.; Suzuki, J.; Oku, T.; Motokawa, R.; Sasao, H.; Tanaka, H.; Yamaguchi, D.; Shimizu, H.; Hashimoto, T. *J. Appl. Crystallogr.* **2007**, *40*, s474.
(28) Koizumi, S.; Iwase, H.; Suzuki, J.; Oku, T.; Motokawa, R.; Sasao, H.; Tanaka, H.; Yamaguchi, D.; Shimizu, H.; Hashimoto, T. *Physica B* **2006**, *385*, 1000.
(29) Rosta, L. *Physica B* **1989**, *156*, 615.
(30) Choi, S.-M.; Barker, J. G.; Glinka, C. J.; Cheng, Y. T.; Gammel, P. L. *J. Appl. Crystallogr.* **2000**, *33*, 793.
(31) Chen, H.; Shen, L.; Wu, C. *Macromolecules* **2006**, *39*, 2325.
(32) Daoud, M.; Cotton, J. P. *J. Phys. (Paris)* **1982**, *43*, 531.
(33) The scattering function of the two-layered core−shell model is expressed by the three-layered core−shell model without the middle region ($N_{NIPAM}^{(m)} = 0$, $R_m = R_c$).
(34) (a) Zhu, P. W.; Napper, D. H. *J. Colloid Interface Sci.* **1994**, *164*, 489. (b) Zhu, P. W.; Napper, D. H. *Colloids Surf., A* **1996**, *113*, 145.
(35) (a) Balamurugan, S.; Mendez, S.; Balamurugan, S. S.; O'Brien II, M. J.; Lopéz, G. P. *Langmuir* **2003**, *19*, 2545. (b) Yim, H.; Kent, M. S.; Satija, S.; Mendez, S.; Balamurugan, S. S.; Balamurugan, S.; Lopéz, G. P. *Phys. Rev. E* **2005**, *72*, 051801.
(36) de Gennes, P. G. *C. R. Acad. Sci., Ser. II* **1991**, *313*, 1117.
(37) Wagner, M.; Brochard-Wyart, F.; Hervet, H.; de Gennes, P. G. *Colloid Polym. Sci.* **1993**, *271*, 621.
(38) (a) Baulin, V. A.; Halperin, A. *Macromol. Theory Simul.* **2003**, *12*, 549. (b) Baulin, V. A.; Zhulina, E. B.; Halperin, A. *J. Chem. Phys.* **2003**, *119*, 10977.
(39) Halperin, A. *Macromolecules* **1987**, *20*, 2943.
(40) Higgins, J. S.; Benoît, H. C. *Polymers and Neutron Scattering*; Oxford University Press: Oxford, 1994.
(41) Pedersen, J. S. *Adv. Colloid Interface Sci.* **1997**, *70*, 171, and references therein.
(42) Sears, V. F. *Neutron News* **1992**, *3*, 26.
(43) Dozier, W. D.; Huang, J. S.; Fetters, L. J. *Macromolecules* **1991**, *24*, 810.
(44) The blob size changes depending on the distance from the origin of the micelle as shown in Figure 2. For simplicity, we assume that the blob size $\xi^{(\alpha)}$ does not depend on the distance. In this case, $\xi^{(\alpha)}$ should be regarded as an average blob size.
(45) Schulz, G. V. *Z. Phys. Chem.* **1939**, *B43*, 25.
(46) Zimm, B. H. *J. Chem. Phys.* **1948**, *16*, 1099.
(47) Ringsdorf, H.; Venzmer, J.; Winnik, F. M. *Macromolecules* **1991**, *24*, 1678.
(48) Nojima, R.; Sato, T.; Qiu, X.; Winnik, F. M. *Macromolecules* **2008**, *41*, 292.
(49) Wang, X.; Wu, C. *Macromolecules* **1999**, *32*, 4299.
(50) Kujawa, P.; Winnik, F. M. *Macromolecules* **2001**, *34*, 4130.
(51) Similar SANS profiles were obtained in a study of a tel-PNIPAM sample of concentration 52 g L^{-1} in the 20 to 30 °C temperature domain. Annaka, M. Private communication.

MA800957Z